Chinese Journal of Natural Medicines

Cytotoxic anthronecyclopentenone heterodimers from the fungus *Penicillium* sp. guided by molecular networking

Ruiyun Huo, Jiayu Dong, Gaoran Liu, Ying Shi, Ling Liu

Citation: Ruiyun Huo, Jiayu Dong, Gaoran Liu, Ying Shi, Ling Liu, Cytotoxic anthronecyclopentenone heterodimers from the fungus *Penicillium* sp. guided by molecular networking, Chinese Journal of Natural Medicines, 2025, 23(10), 1259−1267. doi: 10.1016/S1875−5364(25)60858−2.

View online: https://doi.org/10.1016/S1875−5364(25)60858−2

Related articles that may interest you

Talaketides AG, linear polyketides with prostate cancer cytotoxic activity from the mangrove sediment−derived fungus *Talaromyces* sp. SCSIO 41027

Chinese Journal of Natural Medicines. 2024, 22(11), 1047−1056 https://doi.org/10.1016/S1875−5364(24)60659−X

Rapid identification of stigmastane−type steroid saponins from *Vernonia amygdalina* leaf based on α−glucosidase inhibiting activity and molecular networking

Chinese Journal of Natural Medicines. 2022, 20(11), 846−853 https://doi.org/10.1016/S1875−5364(22)60235−8

Cytotoxic diaporindene and tenellone derivatives from the fungus *Phomopsis lithocarpus*

Chinese Journal of Natural Medicines. 2021, 19(11), 874−880 https://doi.org/10.1016/S1875−5364(21)60095−X

New antibacterial depsidones from an ant−derived fungus *Spiromastix* sp. MY−1

Chinese Journal of Natural Medicines. 2022, 20(8), 627−632 https://doi.org/10.1016/S1875−5364(22)60170−5

Multioxidized polyketides from an endophytic *Penicillium* sp. YUD17006 associated with *Gastrodia elata*

Chinese Journal of Natural Medicines. 2024, 22(11), 1057−1064 https://doi.org/10.1016/S1875−5364(24)60724−7

Four new diphenyl ether derivatives from a mangrove endophytic fungus *Epicoccum sorghinum*

Chinese Journal of Natural Medicines. 2022, 20(7), 537−540 https://doi.org/10.1016/S1875−5364(22)60171−7

Wechat

Chinese Journal of Natural Medicines 23 (2025) 1259-1267

Contents lists available at ScienceDirect

Chinese Journal of Natural Medicines

journal homepage: www.cjnmcpu.com/

Original article

Cytotoxic anthrone–cyclopentenone heterodimers from the fungus *Penicillium* sp. guided by molecular networking

Ruiyun Huo[a,b], Jiayu Dong[a,b], Gaoran Liu[a,b], Ying Shi[a,b], Ling Liu[a,b,*]

[a] *State Key Laboratory of Microbial Diversity and Innovative Utilization, Institute of Microbiology, Chinese Academy of Sciences, Beijing 100101, China*
[b] *University of Chinese Academy of Sciences, Beijing 100049, China*

ARTICLE INFO

Article history:
Received 26 September 2024
Revised 13 December 2024
Accepted 17 December 2024
Available online 20 October 2025

Keywords:
Mangrove-derived fungi
Molecular networking
HSQC-based SMART
Structure elucidation
DP4+ ^{13}C NMR calculation
Cytotoxic activity

ABSTRACT

(±)-Penicithrones A–D (**1a/1b–4a/4b**), four novel pairs of anthrone–cyclopentenone heterodimers characterized by a distinctive bridged 6/6/6–5 tetracyclic core skeleton, together with three previously identified compounds (**5–7**), were isolated from the crude extract of the mangrove-derived fungus *Penicillium* sp., guided by heteronuclear single quantum correlation (HSQC)-based small molecule accurate recognition technology (SMART 2.0) and liquid chromatography-tandem mass spectrometry (LC-MS/MS)-based molecular networking. The structural elucidation of new compounds was accomplished through comprehensive spectroscopic analysis, and their absolute configurations were determined using DP4+ ^{13}C nuclear magnetic resonance (NMR) calculations and electronic circular dichroism (ECD) calculations. Compounds **1a/1b–4a/4b** demonstrated moderate cytotoxicity against three human cancer cell lines HeLa, HCT116 and MCF-7 with half maximal inhibitory concentration (IC_{50}) values ranging from 15.95 ± 1.64 to 28.56 ± 2.59 μmol·L^{-1}.

1. Introduction

Natural products have consistently demonstrated a crucial role in pharmaceutical research, significantly impacting the treatment of human diseases [1–3]. Anthrones represent a class of structurally diverse hybrid natural products exhibiting a broad spectrum of biological activities, including antimicrobial, antioxidative, caspase-3 inhibitory, and cytotoxic properties [4–8]. These compounds are biosynthesized from a polyketide chain containing eight C2 units, which undergo condensation reactions to form the carbon skeleton of anthrones [9]. Anthrone derivatives, particularly those isolated from fungi, occur in complex structures such as dimers and heterodimers. More than 20 anthrone analogues have been isolated and characterized from the genus *Penicillium*, with several demonstrating antifungal activity [8, 10]. These natural products have garnered significant research interest due to their potential applications in medicine and pharmaceuticals.

The strains of *Penicillium* are prevalent in both terrestrial and marine ecosystems [11, 12], and have been identified as a productive source of structurally diverse secondary metabolites including alkaloids, terpenes, isocoumarins, and polyketides, owing to their abundant secondary metabolites biosynthetic gene clusters [13–16]. These compounds demonstrate various bioactivities, including cytotoxic, antiinflammatory, antiviral, *α*-glucosidase inhibitory, antimicrobial, insecticidal, and biocontrol activities [16–19]. Mangrove-derived fungi, inhabiting tropical and subtropical intertidal estuarine zones, represent a promising source of structurally diverse and biologically active secondary metabolites [20–22]. During our ongoing investigation of new bioactive compounds from mangrove-derived fungi [23–25], the fungus *Penicillium* sp. (LA032) was selected for detailed study. The application of heteronuclear single quantum correlation (HSQC)-based small molecule accurate recognition technology (SMART 2.0) and liquid chromatography-tandem mass spectrometry (LC-MS/MS)-based molecular networking methods (Fig. 1) facilitated the targeted isolation and rapid identification of four new pairs of anthrone–cyclopentenone heterodimers, (±)-penicithrones A–D (**1a/1b–4a/4b**) and three known anthrones (**5–7**) (Fig. 2). Compounds **1a/1b–4a/4b** represent the first examples of anthrone–cyclopentenone heterodimers featuring an unprecedented bridged 6/6/6–5 tetracyclic core skeleton. This paper describes the isolation, structure elucidation, and cytotoxic activity evaluation of these compounds.

2. Results and discussion

The ethyl acetate extract was prepared and fractionated by silica gel column chromatography (CC) to yield eight fractions (Frs. 1–8). HSQC-based SMART 2.0 analysis was employed for rapid screening and prediction of natural product skeletal structures [26]. The analysis revealed that four of the top six compounds, ranked by cosine similarity score, were anthraquinones containing aliphatic chain substituents (Fig. 1A). Subsequent isolation was guided by LC-MS/MS-based molecular networking using the Global Natural Products Social (GNPS) web platform [27]. Analysis of Fr. 2 led to the identification of citreorosein (**5**) [28], 2-chloro-1,3,8-trihydroxy-6-(hydroxymethyl)anthracene-9,10-dione (**6**) [29], and endocrocin (**7**) [30]. Notably, the global molecular network ana-

* Corresponding author.
E-mail address: liul@im.ac.cn (L. Liu)

https://doi.org/10.1016/S1875-5364(25)60858-2
Copyright © 2025, China Pharmaceutical University. Published by Elsevier B.V. All rights reserved.

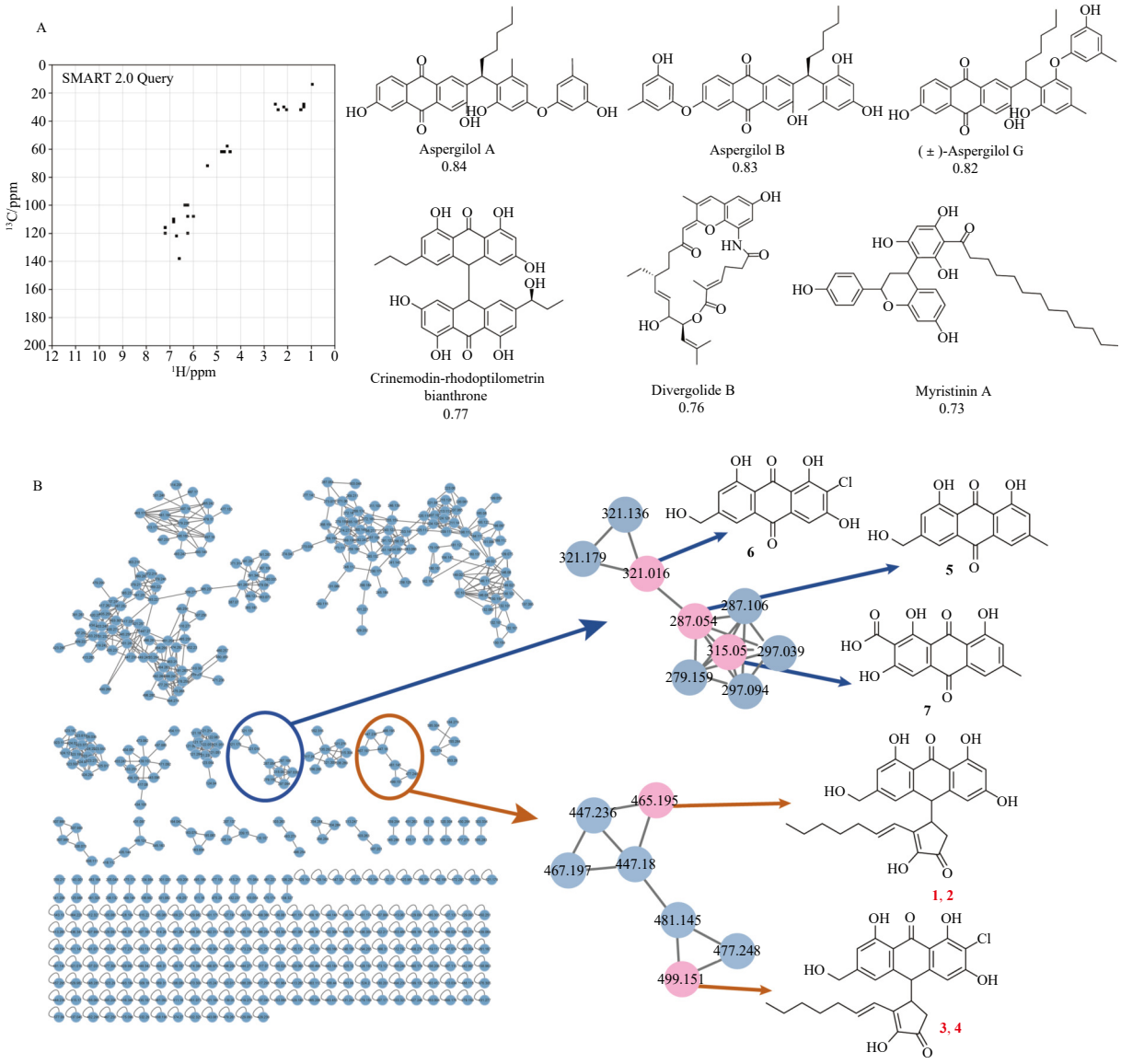

Fig. 1 (A) Digitized HSQC spectrum and the SMART results. (B) Molecular networking analysis.

lysis identified a distinct cluster of compounds with a molecular weight difference of exactly 34 mass units. This finding suggests the presence of novel chlorinated quinone derivatives within the dataset (Fig. 1B). Based on this discovery, targeted separations were conducted to explore and characterize these new compounds.

Penicithrone A (**1**) was isolated as a brown solid. Its molecular formula was determined to be $C_{27}H_{28}O_7$ with fourteen degrees of unsaturation based on the high resolution electrospray ionization mass spectroscopy (HR-ESI-MS) data at *m/z* 465.1904 $[M + H]^+$ (Calcd. for $C_{27}H_{29}O_7$ *m/z* 465.1908). The infrared spectroscopy (IR) spectrum showed strong absorption bands at 3303 and 1682 cm^{-1}, indicating the presence of hydroxy and carbonyl groups, respectively. Analysis of the ^{1}H nuclear magnetic resonance (NMR) data (Table 1) of **1** indicated the presence of two exchangeable protons [δ_H 12.43 (s) and 12.25 (s)], four aromatic protons [δ_H 6.86 (s), 6.74 (d, *J* = 2.0 Hz), 6.55 (s), and 6.34 (d, *J* = 2.0 Hz)], two olefinic protons [δ_H 6.69, d (16.0) and 6.65, dt (16.0, 6.0)], two sp^3 methines [δ_H 4.71 (d, *J* = 2.5 Hz) and 3.58 (dd, *J* = 6.0, 2.5 Hz)], six methylenes [δ_H 4.58 (s), 2.41 (m), 2.03 (overlap), 1.62 (m), 1.57 (d, *J* = 18.0 Hz), 1.41 (m) and 1.34 (m)] and one methyl [δ_H 0.92 (t, *J* = 7.0 Hz)]. The ^{13}C NMR (Table 2) and HSQC spectra revealed 27 carbon resonances including one methyl carbon, six methylenes (one oxygenated), two sp^3 methines, six aromatic or olefinic methine carbons, and twelve sp^2 quarternary carbons including two carbonyl carbons (δ_C 192.3 and 199.1, respectively). These data accounted for all ^{1}H and ^{13}C NMR resonances except for three unobserved exchangeable protons, indicating that **1** was a tetracyclic compound.

The planar structure of **1** was elucidated through comprehensive 2D NMR experiments (Fig. 3). The heteronuclear multiple-bond correlation (HMBC) from H-2 to C-3, C-9 and C-9a, from H-4 to C-2, C-3, C-9a and C-10, from H-5 to C-7, C-8a, C-10a and C-10, from H-7 to C-8a and C-9, from H-10 to C-4a, C-8a, C-9a and C-10a, from OH-1 to C-1, C-2 and C-9a, and from OH-8 to C-7, C-8 and C-8a enabled the determination of the anthrone moiety (rings A–C) with two hydroxy groups positioned at C-1 and C-8, respectively. Additional HMBC from H_2-11 (δ_H 4.58) to C-5, C-6 and C-7 indicated the presence of a hydroxymethyl group (CH_2-11) attached at C-6. The ^{1}H–^{1}H correlated spectroscopy (COSY) cross peaks of H-4′/H_2-5′ and H-6′/H-7′/H_2-8′/H_2-9′/H_2-10′/H_2-11′/H_3-12′, combined with the HMBC from H_2-5′ to C-1′ and C-3′, from H-4′ to C-1′, C-2′ and C-3′, and from the olefinic proton H-6′ to C-2′, C-3′ and C-4′, established the cyclopentenone ring with a 1-heptenyl side chain at C-3′. Furthermore, the ^{1}H–^{1}H COSY cross peak of H-10/H-4′ and the key HMBC from H-10 to C-3′, C-4′ and C-5′, and from H-4′ to C-4a, C-10 and C-10a confirmed the connection between the anthrone moiety and the cyclopentenone

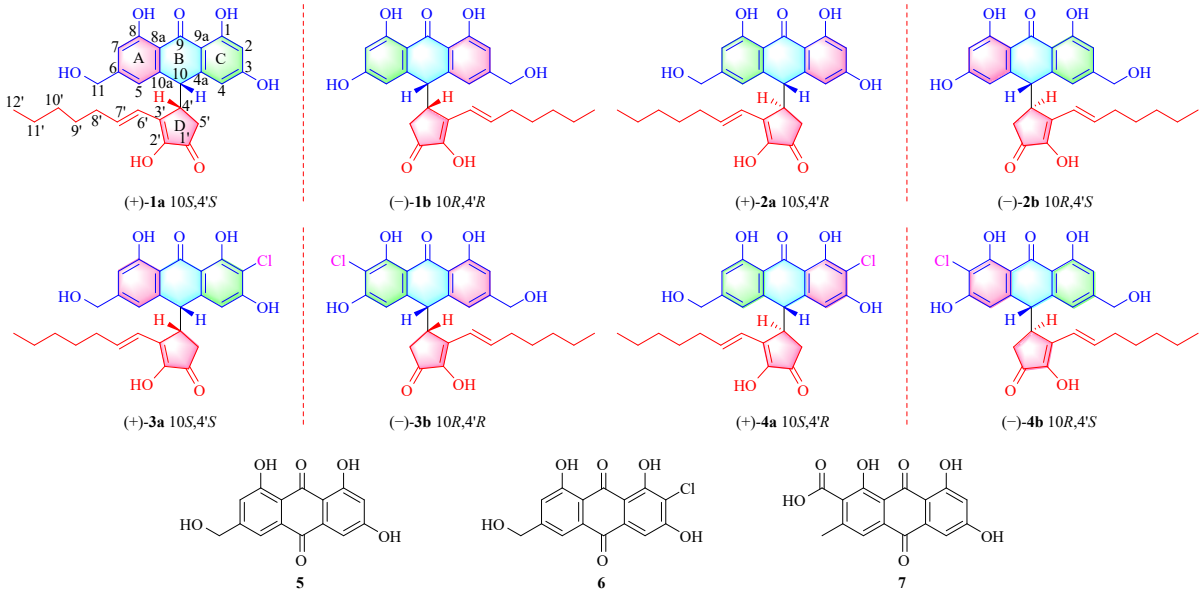

Fig. 2 Chemical structures of compounds (±)-**1**–(±)-**4** and **5**–**7**.

Table 1 ^{1}H NMR (500 MHz) data for **1**–**4** in acetone-d_6.

No.	δ_H (J in Hz)			
	1	**2**	**3**	**4**
2	6.34, d (2.0)	6.27, d (2.0)		
4	6.74, d (2.0)	6.18, d (2.0)	6.93, s	6.36, s
5	6.55, s	7.24, s	6.55, s	7.27, s
7	6.86, s	6.92, s	6.88, s	6.94, s
10	4.71, d (2.5)	4.78, d (2.5)	4.69, d (3.0)	4.79, d (3.0)
11	4.58, s	4.73, s	4.57, s	4.73, s
4′	3.58, dd (6.0, 2.5)	3.63, dd (6.0, 2.5)	3.57, dd (6.0, 3.0)	3.66, dd (6.0, 3.0)
5′a	2.03, overlap	1.96, dd (18.0, 6.0)	1.99, m	1.99, dd (6.0, 18.0)
5′b	1.57, d (18.0)	1.59, m	1.57, m	1.59, m
6′	6.69, d (16.0)	6.71, dt (16.0, 1.5)	6.62, d (16.0)	6.71, dt (16.0, 1.0)
7′	6.65, dt (16.0, 6.0)	6.69, dt (16.0, 6.0)	6.59, dt (16.0, 6.0)	6.70, dt (16.0, 6.0)
8′	2.41, m	2.43, m	2.37, m	2.40, m
9′	1.62, m	1.63, m	1.59, m	1.61, m
10′	1.41, m	1.43, m	1.39, m	1.41, m
11′	1.34, m	1.42, m	1.37, m	1.40, m
12′	0.92, t (7.0)	0.92, t (7.0)	0.89, t (7.0)	0.91, t (7.0)
OH-1	12.43, s	12.41, s	13.10, br s	13.10, s
OH-8	12.25, s	12.29, s	12.14, s	12.13, s

ring *via* a unique C-4′–C-10 linkage, thus establishing an unique bridged 6/6/6–5 tetracyclic core skeleton. The remaining hydroxy groups were positioned at C-2′ and C-3, supported by the chemical shift values for C-2′ (δ_C 151.4) and C-3 (δ_C 166.0), respectively. Thus, the planar structure for **1** was established as shown (Fig. 2).

The *E*-geometry of the C-6′/C-7′ olefin was determined based on large coupling constants ($J_{6',7'}$ = 16.0 Hz). The relative configuration of two adjacent chiral centers (C-10 and C-4′) could not be determined through nuclear Overhauser effect spectroscopy (NOESY) data experiment. To establish the relative configuration of **1**, theoretical calculations of ^{13}C NMR data for the two possible isomers (10*S**,4′*S**)-**1** and (10*R**,4′*S**)-**1** were conducted using the gauge-including atomic orbitals (GIAO) method at the mPW1PW91/6-311 + G (d,p) level. The calculated ^{13}C NMR data of the isomer (10*S**,4′*S**)-**1** demonstrated strong correlation with the experimental ^{13}C NMR data, indicated by a high linear correlation coefficient (R^2). DP4+ probability analyses identified (10*S**,4′*S**)-**1** as the isomer with 100% probability (Fig. 4). The absence of specific rotation or detectable Cotton effects in the ex-

Table 2 ^{13}C NMR (125 MHz) data for **1**–**4** in acetone-d_6.

No.	δ_C, mult			
	1	**2**	**3**	**4**
1	166.3, C	166.2, C	161.3, C	161.3, C
2	102.5, CH	102.7, CH	106.3, C	107.5, C
3	166.0, C	164.8, C	161.1, CH	160.1, C
4	108.9, CH	110.8, CH	108.9, CH	110.6, CH
4a	149.8, C	143.9, C	147.0, C	141.2, C
5	119.3, CH	117.6, CH	119.4, CH	117.8, CH
6	151.5, C	153.2, C	152.0, C	153.7, C
7	114.0, CH	113.7, CH	114.1, CH	113.8, CH
8	163.5, C	163.5, C	163.6, C	163.6, C
8a	115.7, C	115.1, C	115.5, C	114.9, C
9	192.3, C	192.3, C	192.1, C	192.3, CH
9a	110.3, C	110.9, C	110.5, C	111.3, C
10	44.9, CH	44.6, CH	44.7, CH	44.4, CH
10a	140.9, C	146.8, C	147.0, C	146.7, C
11	63.9, CH_2	64.0, CH_2	63.8, CH_2	64.0, CH_2
1′	199.1, C	199.2, C	199.1, C	199.2, C
2′	151.4, C	151.4, C	151.4, C	151.5, C
3′	138.7, C	138.4, C	138.6, C	138.5, C
4′	47.1, CH	46.7, CH	47.0, CH	46.6, CH
5′	34.2, CH_2	34.0, CH_2	34.3, CH_2	34.0, CH_2
6′	123.4, CH	123.3, CH	123.3, CH	123.2, CH
7′	139.2, CH	139.0, CH	139.2, CH	139.0, CH
8′	34.6, CH_2	34.6, CH_2	34.6, CH_2	34.7, CH_2
9′	29.6, CH_2	29.0, CH_2	29.5, CH_2	29.0, CH_2
10′	32.3, CH_2	32.3, CH_2	32.1, CH_2	32.4, CH_2
11′	23.2, CH_2	23.2, CH_2	23.2, CH_2	23.2, CH_2
12′	14.4, CH_3	14.4, CH_3	14.4, CH_3	14.4, CH_3

perimental electronic circular dichroism (ECD) spectrum of **1** indicated its racemic nature. Subsequently, **1** was separated by chiral High-performance liquid chromatography (HPLC) into two enantiomers (+)-**1a** ($[\alpha]_D^{25}$ +22.5) and (−)-**1b** ($[\alpha]_D^{25}$ −10.0). The absolute configurations of (+)-**1a** and (−)-**1b** were established through comparison of the experimental and calculated ECD spectra (Fig. 5) generated by time dependent density functional theory (TD-DFT) for two enantiomers (10*S*,4′*S*)-**1** and (10*R*,4′*R*)-**1**. The experimental ECD spectra of (+)-**1a** and (−)-**1b** corresponded with the calculated spectra of (10*S*,4′*S*)-**1** and (10*R*,4′*R*)-**1**, respectively, enabling definitive assignment of (+)-**1a** as 10*S*,4′*S* and (−)-**1b** as 10*R*,4′*R*.

Penicithrone B (**2**) shared an identical molecular formula ($C_{27}H_{28}O_7$) with penicithrone A (**1**), as determined by HR-ESI-MS data. The IR spectrum of **2** exhibited similar signals to those of **1**. Comparison of the 1D NMR spectroscopic data between **2** and **1** revealed differences in chemical shifts around C-10 and C-4′, suggesting that the primary structural difference lay in the configuration of either C-10 or C-4′. This observation was corroborated by relevant ^{1}H–^{1}H COSY cross peak of H-10/H-4′ and HMBC (Fig. 3) from H-10 to C-3′, C-4′ and C-5′, and from H-4′ to C-4a, C-10 and C-10a. To establish the relative configuration of **2**, calculations of ^{13}C NMR chemical shifts were performed. Both correlation coefficients (R^2) and DP4+ probability analysis (Fig. 6) indicated that **2** possessed the configuration of 10*R**,4′*S**.

Compound **2** was determined to be an enantiomeric mixture based on its baseline ECD curve and negligible optical rotation. Chiral resolution of **2** on a chiral Kromasil 5-CelluCoat column yielded the enantiomers (+)-**2a** and (−)-**2b**. The absolute configurations of these enantiomers were determined through comparison of experimental and calculated ECD spectra (Fig. 5). The calculated ECD curves of (10*S*,4′*R*)-**2** and (10*R*,4′*S*)-**2** demonstrated strong correlation with the experimental spectra of (+)-**2a** and (−)-**2b**, respectively, enabling assignment of the absolute configurations of (+)-**2a** as 10*S*,4′*R* and (−)-**2b** as 10*R*,4′*S*.

The molecular formula of **3** was established as $C_{27}H_{27}ClO_7$ through HR-ESI-MS analysis $[M + H]^+$ *m/z* 499.1522 (Calcd. for $C_{27}H_{28}ClO_7$ *m/z* 499.1518), with an isotopic peak at *m/z* 501.1522 of one-third intensity indicating the presence of a chlorine atom. The ^{13}C NMR spectrum (Table 2) displayed 27 carbon signals, comprising one methyl, six methylenes (one oxygenated), two sp^3 methines, five aromatic or olefinic methine carbons, and thirteen quarternary sp^2 carbons including two carbonyl carbons. The 1D NMR spectral data of **3** showed close similarity to penicithrone A (**1**), with notable differences in the deshielded C-2 ($\Delta\delta_C$ +3.8) and the presence of a singlet aromatic signal at H-4 (δ_H 6.93) in **3**, indicating chlorination of **1**, consistent with their 34 mass unit difference. The chlorine substituent position at C-2 was confirmed through key HMBC (Fig. 3) from H-4 to C-2 (δ_C 106.3), C-3 (δ_C 161.1), C-9a (δ_C 110.5) and C-10 (δ_C 44.7), and OH-1 to C-1 (δ_C 161.3), C-2 and C-9a. Compound **3** was thus characterized as a rare chlorinated anthrone–cyclopentenone heterodimer. The minimal optical rotation and weak Cotton effects indicated that compound **3** existed as enantiomers. Chiral HPLC separation of (±)-**3** yielded (+)-**3a** ($[\alpha]_D^{25}$ +23.3) and (−)-**3b** ($[\alpha]_D^{25}$ −15.8). The experimental ECD spectra of (+)-**3a** and (−)-**3b** exhibited patterns analogous to those of (+)-**1a** and (−)-**1b** (Fig.7) confirming the absolute configurations of (+)-**3a** and (−)-**3b** as 10*S*,4′*S* and 10*R*,4′*R*, respectively (Fig. 2).

(±)-Penicithrone D (**4a**/**4b**) exhibited the same molecular formula of $C_{27}H_{27}ClO_7$ as **3** , as determined by HR-ESI-MS data at *m/z* $[M + H]^+$ 499.1517 (Calcd. for $C_{27}H_{28}ClO_7$ *m/z* 499.1518). The 1D and 2D NMR data (Tables 1 and 2) for **4** demonstrated similarity to those of **3**, suggesting that **4** represented a stereoisomer of **3**, which was subsequently confirmed by ^{1}H–^{1}H COSY and HM-

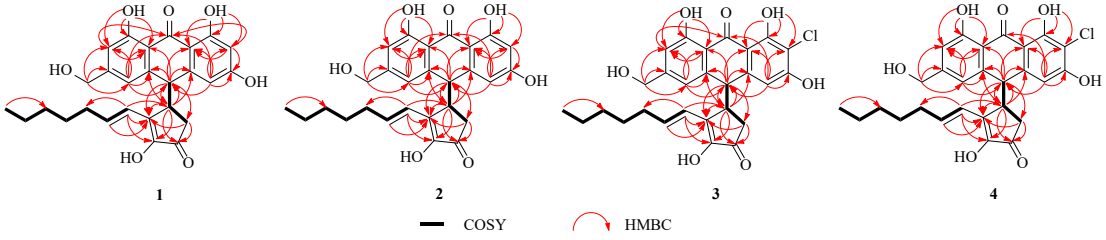

Fig. 3 Key ^{1}H–^{1}H COSY and HMBC of compounds **1**–**4**.

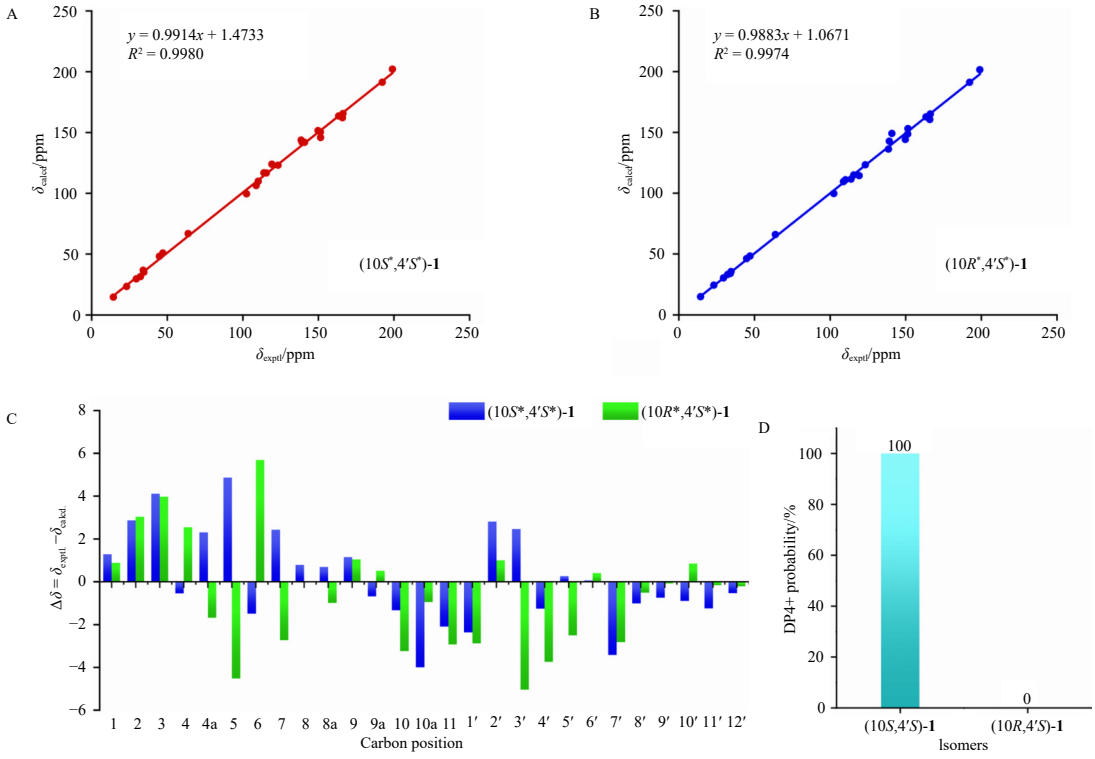

Fig. 4 The ^{13}C NMR calculation results of two plausible isomers of **1**. (A–B) Linear correlation plots of calculated *vs* experimental ^{13}C NMR chemical shifts. (C–D) Relative errors between the calculated ^{13}C NMR chemical shifts the recorded data and DP4+ probability analysis.

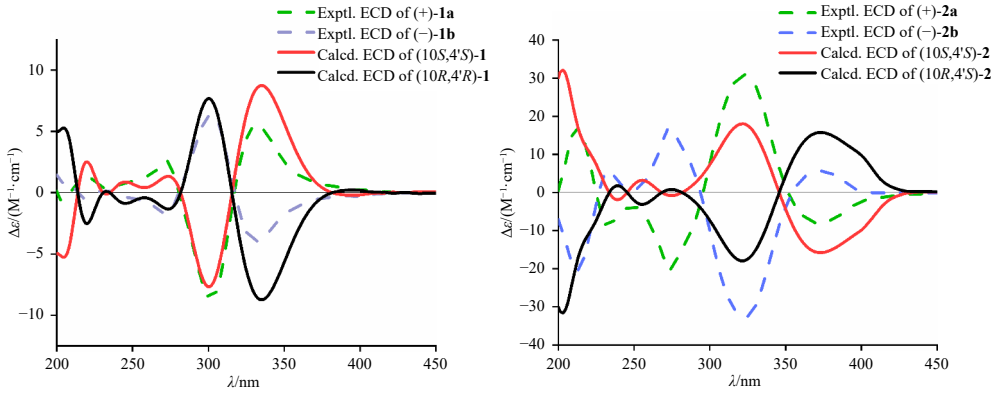

Fig. 5 Calculated and experimental ECD spectra of compounds **1a**/**1b** and **2a**/**2b**.

BC data (Fig. 3). Additionally, **4** underwent separation by chiral HPLC to produce two pure enantiomers (+)-**4a** ($[\alpha]_D^{25}$ +91.9) and (−)-**4b** ($[\alpha]_D^{25}$ −81.1). The absolute configurations of the enantiomers (+)-**4a** and (−)-**4b**, displaying mirror imagelike ECD curves, were determined as 10*S*,4′*R* and 10*R*,4′*S* through comparison with (+)-**2a** and (−)-**2b** (Fig. 7), respectively.

Moreover, based on comparative analysis of NMR data with literature reports, three additional known compounds were identified as citreorosein (**5**) [28], 2-chloro-1,3,8-trihydroxy-6-(hydroxymethyl)anthracene-9,10-dione (**6**) [29] and endocrocin (**7**) [30], respectively.

Compounds **1a**/**1b**–**4a**/**4b** underwent evaluation for cytotoxic activity *in vitro* (Table 3) against human cancer lines HeLa, HCT116 and MCF-7. The compounds demonstrated cytotoxicity with half maximal inhibitory concentration (IC_{50}) values ranging from 15.95 ± 1.64 to 28.56 ± 2.59 μmol·L^{-1}. No significant difference in activity was observed between enantiomers, and among the four pairs of enantiomers, compounds **3a**/**3b** and **4a**/**4b** displayed enhanced activities against cell lines with IC_{50} values ranging from 15.95 ± 1.64 to 21.42 ± 1.38 μmol·L^{-1}.

(±)-Penicithrones A–D (**1**–**4**) constitute the first examples of anthrone–cyclopentenone heterodimers possessing an unprecedented bridged 6/6/6–5 tetracyclic core skeleton, wherein the anthrone moiety connects to the cyclopentenone unit *via* a carbon–carbon bridge bond. In the biosynthetic pathway of anthrone dimers, C–C bond formation primarily occurs on the monomeric backbones through oxidative coupling reactions [8, 9, 31]. Anthrone heterodimers remain exceptionally rare, with reported carbon skeletons limited to anthrone–cyclohexene [6], anthrone–pyranoid diketopiperazine [5], anthrone–anthraquinone and anthrone–*C*-glycosides [32, 33]. Notably, anthrone–cyclopentenone hybrid metabolites featuring the bridged 6/6/6–5 tetracyclic core skeleton have not been previously documented.

Biogenetically, compounds **1**–**4** are hypothesized to originate from two precursors: anthrone (**e** or **f**) and alkyl substituted cyclopentenone (**d**) through a Michael addition reaction (Scheme 1). Intermediate **a**, synthesized from acetyl-CoA and malonyl-CoA by HRPKS through various cyclization and oxida-

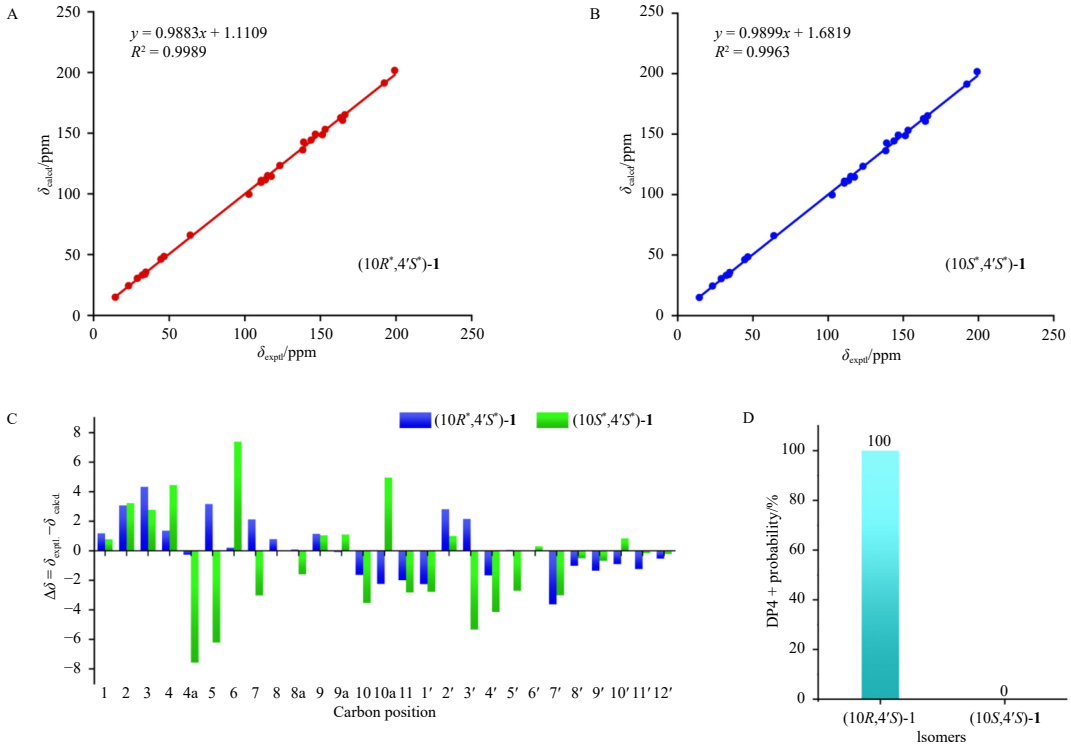

Fig. 6 The ^{13}C NMR calculation results of two plausible isomers of **2**. (A–B) Linear correlation plots of calculated *vs.* experimental ^{13}C NMR chemical shifts. (C–D) Relative errors between the calculated ^{13}C NMR chemical shifts the recorded data and DP4+ probability analysis.

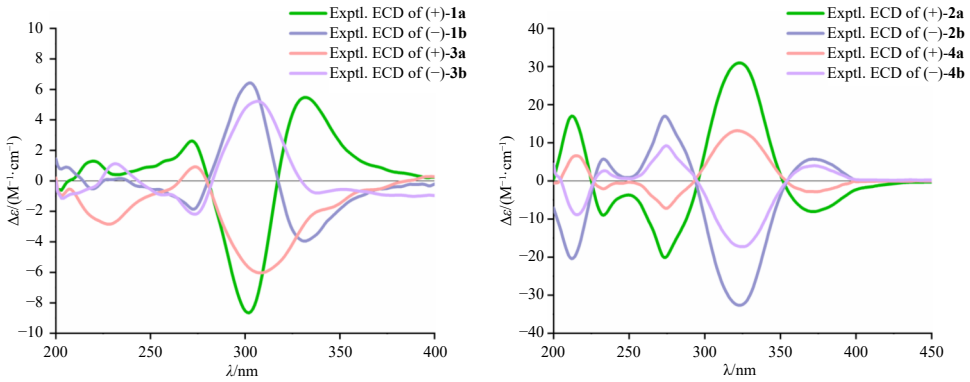

Fig. 7 Experimental ECD spectra of **1**–**4**.

tion reactions, undergoes oxidation to form **b**, followed by rearrangement and ring contraction reactions to produce cyclopentenone (**d**). The anthrone pathway initiates with the synthesis of atrochrysone thioester by NR-PKS and its conversion to atrochrysone carboxylic acid by thioesterase, subsequently diverging into two pathways. In the first pathway, atrochrysone carboxylic acid undergoes dehydration and oxidation to form **7**, which is decarboxylated to emodin, oxidized to **5** , and chlorinated by halogenase to yield **6**. In the second pathway, atrochrysone carboxylic acid is decarboxylated to atrochrysone, followed by dehydration, hydroxylation, and chlorination to form anthrones **e** and **f**. Subsequently, precursors **e** and **f** undergo a Michael addition reaction with precursor **d** to generate compounds **1**–**4**.

3. Conclusion

This investigation utilized HSQC-based SMART strategy and LC-MS/MS-based molecular networking to isolate four novel pairs of anthrone–cyclopentenone heterodimers (±)-penicithrones A–D (**1a**/**1b**–**4a**/**4b**) characterized by a distinctive bridged 6/6/6–5 tetracyclic core skeleton. The newly identified compounds demonstrated cytotoxicity with IC_{50} values ranging from 15.95 ± 1.64 to 28.56 ± 2.59 μmol·L^{-1}. This integrated approach expedites the discovery of novel bioactive compounds while expanding the structural and biological diversity of anthrone heterodimers, presenting promising opportunities for chemical synthesis and medicinal applications.

4. Experimental

4.1. General experimental procedures

Optical rotations were measured on an Anton Paar MCP 200 automatic polarimeter (Anton Paar, Graz, Austria), and ultraviolet (UV) data were obtained on a Thermo Genesys-10S UV/Vis spectrophotometer (Thermo Fisher Scientific, Waltham, MA, USA). IR data were recorded using a Nicolet IS5 FT-IR spectrophotometer (Thermo Fisher Scientific, Waltham, MA, USA). The 1D/2D NMR spectra were collected from a Bruker Avance-500

Table 3 Cytotoxicity of compounds **1a**/**1b**–**4a**/**4b** (mean ± SD. n = 3).

Compound	IC_{50} (μmol·L^{-1})		
	HeLa	HCT116	MCF-7
(+)-**1a**	21.93 ± 2.47	23.22 ± 1.84	22.77 ± 1.80
(−)-**1b**	20.61 ± 0.99	27.86 ± 2.25	27.43 ± 3.30
(+)-**2a**	21.66 ± 2.65	20.84 ± 1.63	21.07 ± 2.06
(−)-**2b**	22.87 ± 1.48	25.92 ± 1.77	28.56 ± 2.59
(+)-**3a**	18.42 ± 0.19	20.35 ± 1.09	21.24 ± 0.93
(−)-**3b**	19.51 ± 1.91	21.42 ± 1.38	20.63 ± 1.76
(+)-**4a**	16.29 ± 1.48	15.95 ± 1.64	16.13± 0.53
(−)-**4b**	17.57 ± 0.89	16.42 ± 2.12	16.96 ± 0.72
Cisplatin	8.26 ± 1.83	9.41 ± 1.85	9.00 ± 1.94

spectrometer (Bruker, Bremen, Germany) using solvent signals (acetone-d_6:δ_H 2.05/δ_C 29.8, 206.1) as references. HR-ESI-MS data were obtained using an Agilent Accurate-Mass-Q-TOF LC/MS 6520 instrument (Agilent Technologies, Santa Clara, CA, USA). HPLC separations were performed on an Agilent 1260 instrument equipped with a variable-wavelength UV detector using a Fisher Wharton xbridge C_{18} (10 mm × 250 mm, 5 μm, 2 mL·min^{-1}). Open CC was performed on silica gel (Qingdao Haiyang Chemical Co., Ltd., Qingdao, China), octadecylsilyl (ODS, 50 μm, YMC Co., Ltd., Japan) and Sephadex LH–20 (Amersham Biosciences, Uppsala, Sweden).

4.2. Fungal material and fermentation

The fungal strain *Penicillium* sp. (LA032) was isolated from the rhizospheric soil of a mangrove ecosystem collected from Sanya, China. The strain was identified through phylogenetic analysis based on ITS sequence (GenBank Accession No. OP804236) and morphological observation. The voucher specimen was deposited in the Institute of Microbiology, Chinese Academy of Sciences, Beijing.

The strain *Penicillium* sp. (LA032) was cultivated on potato dextrose agar (PDA) at 25 °C for 7 d. Subsequently, small agar plug pieces were inoculated into 500 mL Fernbach flasks containing 150 mL of media (0.4% glucose, 1% malt extract, and 0.4% yeast extract) at room temperature on an orbital shaker at 150 r·min^{-1} for 4 d to obtain the seed culture. Static fermentation was conducted at 25 °C for 30 d in 30 × 1 L Erlenmeyer flasks containing 200 g of rice and 200 mL of distilled water.

4.3. Extraction and SMART-guided isolation

The fermented rice material underwent repeated extraction with EtOAc (4 × 5.0 L), and the organic solvent was evaporated to dryness, yielding the crude extract (51.0 g). The extract was fractionated through silica gel CC using petroleum ether (PE)/EtOAc gradient elution to produce eight fractions Frs. 1–8. Subsequently, small quantities of fractions (25 mg) were transferred into NMR tubes. HSQC experiments were performed through CSV data files uploaded to the SMART system (http://smart.ucsd.edu/classic). Analysis of Fr. 2 revealed that four of the top six compounds, ranked by cosine similarity score, were anthraquinones with aliphatic chain substituents (Fig. 1A). Based on the SMART positioning results, Fr. 2 demonstrated richness in anthraquinones featuring aliphatic chains and was therefore systematically investigated for its chemical constituents.

Fr. 2 (2.1 g) eluted with 30% EtOAc was separated by ODS CC (20%–100% MeOH/H_2O) to yield nine subfractions Fr. 2.1–Fr. 2.9. Fr. 2.3 (65.3 mg) eluted with 50% MeOH/H_2O was further purified by RP-HPLC (55% MeOH/H_2O for 20 min; 2.0 mL·min^{-1}) to afford compounds **5** (5.2 mg, t_R 13.5 min) and **6** (1.0 mg, t_R 17.5 min). Fr. 2.5 (30.5 mg) eluted with 55% MeOH/H_2O was further purified by RP-HPLC (30%–85% MeOH/H_2O for 45 min; 2.0 mL·min^{-1}) to give compound **7** (4.1 mg, t_R 23.4 min). Fr. 2.6 (23 mg) eluted with 70% MeOH/H_2O was further purified by RP-HPLC (75% MeOH/H_2O for 60 min; 2.0 mL·min^{-1}) to yield compounds **1** (4.2 mg, t_R 41.0 min), **2** (3.1 mg, t_R 46.0 min), **3** (2.8 mg, t_R 52.0 min) and **4** (1.8 mg, t_R 54.0 min).

Compounds **1**–**4** were isolated as racemates. Compound **1**

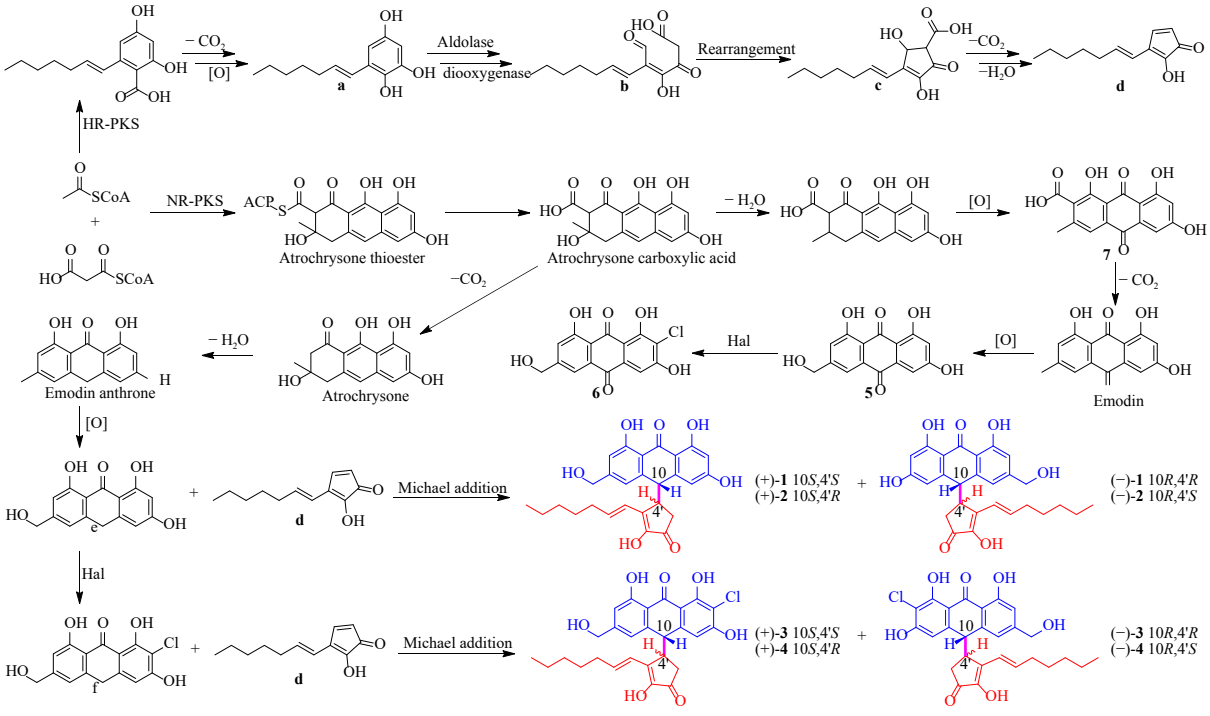

Scheme 1 Putative biosynthetic pathway of compounds (±)-**1**–(±)-**4** and **5**–**7**.

was separated using chiral HPLC column (Kromasil 5-CelluCoat column, 250 × 4.6 mm, 5 μm) with CH_3CN/H_2O (*V*/*V*, 35∶65; flow rate: 0.5 mL·min^{-1}) as the mobile phase, yielding (+)-**1a** (0.8 mg, t_R 83.5 min) and (–)-**1b** (0.7 mg, t_R 84.8 min). Compound **2** was separated using chiral-phase HPLC column (Kromasil 5-CelluCoat column, 250 mm × 4.6 mm, 5 μm) with CH_3CN/H_2O (*V*/*V*, 50∶50; flow rate: 0.5 mL·min^{-1}) as the mobile phase, yielding (+)-**2a** (0.9 mg, t_R 24.5 min) and (–)-**2b** (1.5 mg, t_R 22.0 min). Similarly, (+)-**3a** (0.5 mg, t_R 48.0; min) and (–)-**3b** (0.4 mg, t_R 46.5 min) were obtained using Kromasil 5-CelluCoat column (CH_3CN/H_2O, *V*/*V*, 40∶60, flow rate 0.5 mL·min^{-1}). (+)-**4a** (1.1 mg, t_R 33.0 min) and (–)-**4b** (1.3 mg, t_R 30.0 min) were obtained using Kromasil 5-CelluCoat column (CH_3CN/H_2O, *V*/*V*, 50∶50, flow rate 0.5 mL·min^{-1}).

(±)-Penicithrone A (**1**): brown solid; UV (MeOH) λ_{max} (log ε) 210 (2.75), 300 (2.60) nm, 360 (2.41) nm; IR (neat) ν_{max} 3303, 2928, 1682, 1621, 1384, 1037, 847 cm^{-1}; ^{1}H NMR (500 MHz, acetone-d_6) and ^{13}C NMR data (125 MHz, acetone-d_6), see Tables 1 and 2; HR-ESI-MS at *m/z* 465.1904 [M + H]$^+$ (Calcd. for $C_{27}H_{29}O_7$ *m/z* 465.1908).

(+)-**1a**: $[\alpha]_D^{25}$ +22.5 (*c* 0.04, MeOH); ECD (2.2 × 10^{-4} mol·L^{-1}, MeOH) λ_{max} ($\Delta\varepsilon$) 272 (+2.71), 302 (–8.74).

(–)-**1b**: $[\alpha]_D^{25}$ –10.0 (*c* 0.03, MeOH); ECD (2.2 × 10^{-4} mol·L^{-1}, MeOH) λ_{max} ($\Delta\varepsilon$) 272 (–1.85), 302 (+6.42).

(±)-Penicithrone B (**2**): brown solid; UV (MeOH) λ_{max} (log ε) 210 (2.76), 300 (2.59) nm, 360 (2.47) nm; IR (neat) ν_{max} 3301, 2928, 1689, 1621, 1481, 1025, 848 cm^{-1}; ^{1}H NMR (500 MHz, acetone-d_6) and ^{13}C NMR data (125 MHz, acetone-d_6), see Tables 1 and 2; HR-ESI-MS at *m/z* 465.1913 [M + H]$^+$ (Calcd. for $C_{27}H_{29}O_7$ *m/z* 465.1908).

(+)-**2a**: $[\alpha]_D^{25}$ +88.9 (*c* 0.1, MeOH); ECD (2.2 × 10^{-4} mol·L^{-1}, MeOH) λ_{max} ($\Delta\varepsilon$) 212 (+17.46), 233 (–9.38), 275 (–20.08), 318 (+29.94).

(–)-**2b**: $[\alpha]_D^{25}$ –77.9 (*c* 0.1, MeOH); ECD (2.2 × 10^{-4} mol·L^{-1}, MeOH) λ_{max} ($\Delta\varepsilon$) 212 (–20.79), 233 (+6.07), 275 (+16.94), 318 (–31.61).

(±)-Penicithrone C (**3**): brown solid; UV (MeOH) λ_{max} (log ε) 210 (2.44), 300 (2.29), 360 (2.20) nm; IR (neat) ν_{max} 3352, 2928, 1690, 1612, 1397, 1024, 825 cm^{-1}; ^{1}H NMR (500 MHz, acetone-d_6) and ^{13}C NMR data (125 MHz, acetone-d_6), see Tables 1 and 2; HR-ESI-MS at *m/z* 499.1522 [M + H]$^+$ (Calcd. for $C_{27}H_{28}ClO_7$ *m/z* 499.1518).

(+)-**3a**: $[\alpha]_D^{25}$ +23.3 (*c* 0.04, MeOH); ECD (3.7 × 10^{-4} mol·L^{-1}, MeOH) λ_{max} ($\Delta\varepsilon$) 272 (+0.23), 302 (–1.43).

(–)-**3b**: $[\alpha]_D^{25}$ –15.8 (*c* 0.03, MeOH); ECD (5.0 × 10^{-4} mol·L^{-1}, MeOH) λ_{max} ($\Delta\varepsilon$) 272 (–2.19), 302 (+5.01).

(±)-Penicithrone D (**4**): brown solid; UV (MeOH) λ_{max} (log ε) 210 (2.54), 300 (2.30), 360 (2.21) nm; IR (neat) ν_{max} 3341, 2928, 1690, 1613, 1396, 1025, 825 cm^{-1}; ^{1}H NMR (500 MHz, acetone-d_6) and ^{13}C NMR data (125 MHz, acetone-d_6), see Tables 1 and 2; HR-ESI-MS at *m/z* 499.1517 [M + H]$^+$ (Calcd. for $C_{27}H_{28}ClO_7$ *m/z* 499.1518).

(+)-**4a**: $[\alpha]_D^{25}$ +91.9 (*c* 0.1, MeOH); ECD (1.0 × 10^{-4} mol·L^{-1}, MeOH) λ_{max} ($\Delta\varepsilon$) 212 (+5.99), 233 (–2.09), 275 (–7.21), 318 (+12.86).

(–)-**4b**: $[\alpha]_D^{25}$ –81.1 (*c* 0.1, MeOH); ECD (1.0 × 10^{-4} mol·L^{-1}, MeOH) λ_{max} ($\Delta\varepsilon$) 212 (–7.68), 233 (+2.63), 275 (+9.20), 318 (–16.25).

4.4. LC-MS/MS and molecular networking analysis

LC-MS/MS analyses were conducted using an Agilent series 1260 Infinity HPLC instrument with a Fisher Wharton xbridge C_{18} column (250 mm × 4.60 mm). The mobile phase comprised 0.1% formic acid in H_2O (A) and HPLC-grade MeCN (B). The elution gradient conditions for the LC mobile phase were as follows: 0–5 min, 90%–60% A; 5–20 min, 60%–45% A; 20–40 min, 45% A; 40–50 min, 45/5–0% A. The flow rate of the mobile phase was 1.0 mL·min^{-1}. A molecular net work was generated on the GNPS (http://gnps.ucsd.edu) online workflow. The final results were visualized using Cytoscape 3.6.1.

4.5. NMR calculations

Boltzmann-population exceeding 1% (the relative energy within 3.0 kcal·mol^{-1}) were obtained. Subsequently, the conformers were re-optimized at the M062X/6-31G (d) level using Gaussian 09. Two possible isomers underwent ^{13}C NMR chemical shift calculations using the GIAO method at the mPW1PW91/6-311 + G (d,p) level of theory for DP4+ calculations. The calculated chemical shifts (δ_{calcd}) for each compound were weighted according to the Boltzmann distributions over the conformers. The overall theoretical NMR data were analyzed using linear regression and DP4+ probability.

4.6. ECD calculations

Conformational analyses for four stable conformers were performed using Maestro 10.2 in the OPLS3 molecular mechanics force-field within an energy window of 3.0 kcal·mol^{-1}. All conformers were further optimized by the DFT methods at the B3LYP/6-31G (d) level in the Gaussian 09 software package, respectively. The TD-DFT methods at the B3LYP/6-31G (d) were applied to calculate the 60 lowest electronic transitions, which obtained conformers in vacuum, respectively. The Gaussian function was applied to simulate the ECD spectrum of the conformers. The calculated ECD spectra were obtained according to the Boltzmann weighting of each conformer's ECD spectrum in MeOH solution.

4.7. Cytotoxic assay

Cytotoxic assay was conducted according to previously established protocols [25]. The human cervical cancer cells HeLa (ATCC CCL-2), human colorectal carcinoma cells HCT116 (ATCC CCL-247), and human breast cancer cell line MCF-7 (ATCC HTB-22) were obtained from ATCC. Cells were plated in a 96-well plate and incubated for 12 h. Following incubation, the medium was removed, and each well received 100 μL of medium containing 0.1% DMSO or appropriate concentrations of the test compounds. DMSO served as the negative control. Cisplatin (Lot: K2314537; ≥ 99.5%) was utilized as the positive control. After 48 h incubation at 37 °C, cell proliferation was evaluated by adding 20 μL of MTS reagent to each well, followed by an additional 90 min incubation at 37 °C. The absorbance was measured at 490 nm, with all conditions tested in triplicate.

Funding

This work was supported by the National Key Research and Development Program of China (No. 2022YFC2303100) and the National Natural Science Foundation of China (Nos. 32022002 and 21977113).

Supplementary materials

Experimental details and spectroscopic data of **1a**/**1b**–**4a**/**4b** were provided. Supplementary material related to this article can be requested by sending E-mail to the corresponding author.

Declaration of competing interest

These authors have no conflict of interest to declare.

References

1 Luo ZW, Yin FC, Wang XB, et al. Progress in approved drugs from natural product resources. *Chin J Nat Med*. 2024;22(3):195-211. https://doi.org/10.1016/S1875-5364(24)60582-0.

2 Shi Y, Ji MH, Dong JY, et al. New bioactive secondary metabolites from fungi: 2023. *Mycology*. 2024;15(3):283-321. https://doi.org/10.1080/21501203.2024.2354302.

3 David JN, Gordon MC. Natural products as sources of new drugs over the nearly four decades from 01/1981 to 09/2019. *J Nat Prod*. 2020;83(3):770-803. https://doi.org/10.1021/acs.jnatprod.9b01285.

4 Du L, Zhu T, Fang Y, et al. Aspergiolide A, a novel anthraquinone derivative with naphtho [1,2,3-*de*] chromene-2, 7-dione skeleton isolated from a marine-derived fungus *Aspergillus glaucus*. *Tetrahedron*. 2007;63(5):1085-1088. https://doi.org/10.1016/j.tet.2006.11.074.

5 Chen GD, Bao YR, Huang YF, et al. Three pairs of variecolortide enantiomers from *Eurotium* sp. with caspase-3 inhibitory activity. *Fitoterapia*. 2014;92:252-259. https://doi.org/10.1016/j.fitote.2013.11.012.

6 Zhong WM, Wang JF, Wei XY, et al. Variecolortins A–C, three pairs of spirocyclic diketopiperazine enantiomers from the marine-derived fungus *Eurotium* sp. SCSIO F452. *Org Lett*. 2018;20(15):4593-4596. https://doi.org/10.1021/acs.orglett.8b01880.

7 Anisha C, Sachidanandan P, Radhakrishnan EK. Endophytic *Paraconiothyrium* sp. from *Zingiber officinale* Rosc. displays broad-spectrum antimicrobial activity by production of danthron. *Curr Microbiol*. 2018;75(3):343-352. https://doi.org/10.1007/s00284-017-1387-7.

8 Elbanna AH, Khalil ZG, Bernhardt PV, et al. Neobulgarones revisited: anti and syn bianthrones from an Australian mud dauber wasp nest-associated fungus, *Penicillium* sp. CMB-MD22. *J Nat Prod*. 2021;84(3):762-770. https://doi.org/10.1021/acs.jnatprod.0c01035.

9 Han YB, Bai W, Ding CX, et al. Intertwined biosynthesis of skyrin and rugulosin A underlies the formation of cage-structured bsanthraquinones. *J Am Chem Soc*. 2021;143(35):14218-14226. https://doi.org/10.1021/jacs.1c05421.

10 Morehouse NJ, Flewelling AJ, Johnson JA, et al. Halogenated bianthrones from *Penicillium roseopurpureum*: a fungal endophyte of the marine alga *Petalonia fascia*. *Nat Prod Commun*. 2020;15(1):1-4. https://doi.org/10.1177/1934578x20901405.

11 Petersen C, Sørensen T, Nielsen MR, et al. Comparative genomic study of the *Penicillium* genus elucidates a diverse pangenome and 15 lateral gene transfer events. *IMA Fungus*. 2023;14(1):3. https://doi.org/10.1186/s43008-023-00108-7.

12 Houbraken J, Kocsubé S, Visagie CM, et al. Classification of *Aspergillus*, *Penicillium*, *Talaromyces* and related genera (*Eurotiales*): an overview of families, genera, subgenera, sections, series and species. *Stud Mycol*. 2020;95:5-169. https://doi.org/10.1016/j.simyco.2020.05.002.

13 Li HL, Xu R, Li XM, et al. Simpterpenoid A, a meroterpenoid with a highly functionalized cyclohexadiene moiety featuring gem-propane-1,2-dione and methylformate groups, from the mangrove-derived *Penicillium simplicissimum* MA-332. *Org Lett*. 2018;20(5):1465-1468. https://doi.org/10.1021/acs.orglett.8b00327.

14 Li HT, Yang RN, Xie F, et al. Multioxidized polyketides from an endophytic *Penicillium* sp. YUD17006 associated with *Gastrodia elata*. *Chin J Nat Med*. 2024;22(11):1057-1064. https://doi.org/10.1016/S1875-5364(24)60724-7.

15 Meng LH, Wang CY, Mándi A, et al. Three diketopiperazine alkaloids with spirocyclic skeletons and one bisthiodiketopiperazine derivative from the mangrove-derived endophytic fungus *Penicillium brocae* MA-231. *Org Lett*. 2016;18(20):5304-5307. https://doi.org/10.1021/acs.orglett.6b02620.

16 Zhang X, Yin Q, Li X, et al. Structures and bioactivities of secondary metabolites from *Penicillium* genus since 2010. *Fitoterapia*. 2022;163:105349. https://doi.org/10.1016/j.fitote.2022.105349.

17 Qiu P, Cai RL, Lin L, et al. Three new isocoumarin derivatives from the mangrove endophytic fungus *Penicillium* sp. YYSJ-3. *Chin J Nat Med*. 2020;18(4):256-260. https://doi.org/10.1016/S1875-5364(20)30031-5.

18 Liu S, Su M, Song SJ, et al. An anti-inflammatory PPAR-γ agonist from the jellyfish-derived fungus *Penicillium chrysogenum* J08NF-4. *J Nat Prod*. 2018;81(2):356-363. https://doi.org/10.1021/acs.jnatprod.7b00846.

19 Cheng X, Liang X, Zheng ZH, et al. Penicimeroterpenoids A–C, meroterpenoids with rearrangement skeletons from the marine-derived fungus *Penicillium* sp. SCSIO 41512. *Org. Lett*. 2022;22(16):6330-6333. https://doi.org/10.1021/acs.orglett.0c02160.

20 Carroll AR, Copp BR, Grkovic T, et al. Marine natural products. *Nat Prod Rep*. 2024;41(2):162-207. https://doi.org/10.1039/d3np00061c.

21 Chen SH, Cai RL, Liu ZM, et al. Secondary metabolites from mangrove-associated fungi: source, chemistry and bioactivities. *Nat Prod Rep*. 2022;39(3):560-595. https://doi.org/10.1039/d1np00041a.

22 Zhu JJ, Huang QS, Liu SQ, et al. Four new diphenyl ether derivatives from a mangrove endophytic fungus *Epicoccum sorghinum*. *Chin J Nat Med*. 2022;20(7):537-540. https://doi.org/10.1016/S1875-5364(22)60171-7.

23 Lu PY, Shi Y, Zhang JX, et al. New prenylated indole-benzodiazepine-2, 5-diones with α-glucosidase inhibitory activities from the mangrove-derived *Aspergillus spinosus*. *Int J Biol Macromol*. 2024;257:128808. https://doi.org/10.1016/j.ijbiomac.2023.128808.

24 Huo RY, Zhang JX, Niu SB, et al. New prenylated indole diketopiperazine alkaloids and polyketides from the mangrove-derived fungus *Penicillium* sp. *Front Mar Sci*. 2022;9:1097594 https://doi.org/10.3389/fmars.2022.1097594.

25 Shi Y, Sun XQ, Zhang JX, et al. New cytotoxic γ-Lactam alkaloids from the mangrove-derived fungus *Talaromyces hainanensis* sp. nov. guided by molecular networking strategy. *J Agric Food Chem*. 2024;72(31):17431-17443. https://doi.org/10.1021/acs.jafc.4c03959.

26 Reher R, Kim HW, Zhang C, et al. A convolutional neural network-based approach for the rapid annotation of molecularly diverse natural products. *J Am Chem Soc*. 2020;142(9):4114-4120. https://doi.org/10.1021/jacs.9b13786.

27 Watrous J, Roach P, Alexandrov T, et al. Mass spectral molecular networking of living microbial colonies. *Proc Natl Acad Sci USA*. 2012;109(26):E1743-E1752. https://doi.org/10.1073/pnas.1203689109.

28 Liang JL, Cha HC, Lee SH, et al. A facile synthesis of emodin derivatives, emodin carbaldehyde, citreorosein, and their 10-deoxygenated derivatives and their inhibitory activities on μ-calpain. *Arch Pharm Res*. 2012;35(3):447-454. https://doi.org/10.1007/s12272-012-0307-4.

29 Yamamoto Y, Kiriyama N, Arahata S. Studies on the metabolic products of *Aspergillus fumigatus* (J-4) chemical structure of metabolic products. *Chem Pharm Bull*. 1968;16(2):304-310. https://doi.org/10.1248/cpb.16.304.

30 Yang YC, Lim MY, Lee HS. Emodin isolated from *Cassiaobtusifolia* (Leguminosae) seed shows larvicidal activity against three mosquito species. *J Agric Food Chem*. 2003;51(26):7629-7631. https://doi.org/10.1021/jf034727t.

31 Mai LP, Guéritte F, Dumontet V, et al. Cytotoxicity of rhamnosylanthraquinones and rhamnosylanthrones from *Rhamnus nepalensis*. *J Nat Prod*. 2001;64(9):1162-1168. https://doi.org/10.1021/np010030v.

32 Carroll AR, Nash BD, Duffy S, et al. Albopunctatone, an antiplasmodial anthrone-anthraquinone from the Australian ascidian *Didemnum albopunctatum*. *J Nat Prod*. 2012;75(6):1206-1209. https://doi.org/10.1021/np300074z.

33 Koyama Y, Yamaguchi R, Suzuki K. Total synthesis and structure assignment of the anthrone *C*-glycoside cassialoin. *Angew Chem Int Ed Engl*. 2008;47(6):1084-1087. https://doi.org/10.1002/anie.200704625.